Int. J. Electrochem. Sci., 9 **(2014)** 7552 - 7573

International Journal of ELECTROCHEMICAL SCIENCE
www.electrochemsci.org

Case study: Impact of Amine Containing Organic Compound on the Corrosion and Electrochemical Behaviors of Constructive Alloys in Linear Alpha Olefin Environment

Mohammed A. Amin[1,2,*], *Q. Mohsen*[1], *Nasser Y. Mostafa*[1,3], *Abdullah Al-Refaie*[4], *Avtandil K. Bairamov*[4], *Saad Al-Maaesab*[5], *Esteban Morales Murillo*[5], *Saad Ayed Al-Qahtani*[6]

[1]Materials and Corrosion Lab, Chemistry Department, Faculty of Science, Taif University, 888 Hawiya, Saudi Arabia

[2] Chemistry Department, Faculty of Science, Ain Shams University, P.O. Box 11566, Abbassia, Cairo, Egypt.

[3] Chemistry Department, Faculty of Science, Suez Canal University, Ismailia, Egypt

[4]Corporate Research and Innovation Center (CRI), Saudi Basic Industries Corporation (SABIC), P.O. Box 4545-4700, Thuwal 23955-6900, Saudi Arabia

[5] Materials and Corrosion Section, SABIC Technology Center, P.O. Box #11669, Jubail Industrial City 31961, Saudi Arabia

[6]LAO Operation Department, Jubail United Petrochemical Company, P.O. Box: 10085, Jubail Industrial City 31961, Saudi Arabia

[*]E-mail: maaismail@yahoo.com

Received: 13 July 2014 / *Accepted:* 7 October 2014 / *Published:* 28 October 2014

The impact of a high molecule organic compound containing amine fragment (HMoA) on the corrosion and electrochemical behaviors of carbon steel (CSA516), ferritic (SS410) and austenitic (SS304L) stainless steels was studied in the environment of the LAO (linear α-olefin) plant. Corrosion tests were carried out at 270 ^{o}C and 29 bar in an autoclave at different exposure time intervals (up to 30 days). Corrosion rates were determined using mass losses of the samples with and without HMoA. Optical microscopy (OM) and scanning electron microscopy (SEM) were employed to assess the morphologies of the corroded and inhibited surfaces. Efficiency and kinetics of electrode processes in the presence of HMoA were investigated by means of polarization and impedance measurements. Results of these experimental data are widely presented and discussed in this paper. It was found that the inhibition performance of the tested compound recorded inhibition efficiencies of 30%, 66% and 95% for CSA516, SS410, and SS304L, respectively. Based on the obtained experimental findings and surface examinations and analysis, the mechanism of the inhibition process is discussed.

Keywords: Corrosion; Carbon steel; Stainless steel; Monitoring rates of corrosion; Electrochemical techniques; Surface morphology

1. INTRODUCTION

In the past few years, the industry has concentrated its efforts on minimizing corrosion failures and related costs [1]. Several approaches, including, coatings [2-9], cathodic protection [10-13] and corrosion inhibitors [1,14,15-23] have been employed to mitigate corrosion. The key corrosion control methods also include the use of corrosion-resistant alloys, the use of corrosion monitoring techniques, and the implementation of planned maintenance.

Corrosion-resistant alloys are gaining a widespread acceptance in the chemical industry. Although these alloys are more expensive than carbon steel, they can prevent high failure costs in the long run. Corrosion monitoring techniques are implemented in process streams in order to ensure the integrity of the equipment. Planned maintenance consists of scheduled shutdown periods in order to inspect all equipment and to refurbish or replace equipment that has failed due to corrosion or other mechanisms. Shutdown periods are generally scheduled in advance and are short in duration in order to minimize inspection costs and production losses. Many chemical companies are using risk-based inspection procedures to minimize the likelihood of failure in pressure equipment or equipment containing hazardous materials. Such models determine the risk level on high-risk equipment based on the consequences and propensity to failure.

Earlier, the corrosion behavior of three constructive materials namely carbon steel (SA516), ferritic (410) and austenitic (304L) stainless steels was studied in linear alpha olefin (LAO) environment [24]. The most severe corrosion damage was found for carbon steel. The lowest corrosion rate was determined for stainless steel 304L.

It was practically interesting to investigate here the impact of HMoA on the corrosion and electrochemical behaviors of the above mentioned materials in LAO environment. Measurements were conducted employing chemical and electrochemical studies, complemented with OM, SEM/EDS, and AFM examinations.

2. EXPERIMENTAL

2.1. Materials and Solutions

The tested samples employed in this work are carbon steel (A516-70) and stainless steels (410 SS and SS304L) of chemical composition presented in Table 1. Bulk solution and solution containing high molecular organic compound with amine fragment (HMoA) were provided by plant for lab test.

Table 1. Chemical composition of the three tested steel samples.

Alloy	Alloying elements (%)					
	C	Si	Mn	Cr	Ni	Fe
CSA516-70	0.18	0.13	0.18	0.00	0.00	bal.
SS410	0.15	0.48	0.35	12.59	0.50	bal.
SS304L	0.03	0.46	0.73	18.43	7.91	bal.

2.2. Corrosion tests

The high temperature (270°C and 29 bar) corrosion test of the three tested alloys, were performed in a Teflon-lined steel Autoclave of 400 cm^3 capacity equipped with magnetic stirrer and heat controller. The shape and full design of that Autoclave is presented elsewhere [24]. The corrosion rate determination methodology is the same as in previously published article [24].

Rates of corrosion for each tested sample were calculated based on the mass changes (mass loss) in bulk solution and in the presence of HMoA. Mass loss measurements and removing (cleaning) of corrosion products were performed in a manner consistent with the ASTM G1 [25].

A solution containing 0.5 L HCl (sp gr 1.19) + 3.5 g hexamethylene tetramine + 1L H_2O was used to remove corrosion product [25].

2.3. Electrochemical measurements

For electrochemical measurements and surface analysis, sheets of dimensions (0.7 cm) x (1.5 cm) x (0.25 cm; thickness) were cut from the coupons of the three employed alloys. Prior to electrochemical measurements, all sides of the sheets were isolated to offer an active flat rectangular shaped surface of (0.7 x 0.25 = 0.175 cm^2), immersed into the test solution.

Open circuit potential (OCP) *vs.* time (up 24 hrs), linear polarization resistance (LPR), Tafel plots, cyclic polarization, and ac impedance measurements are the electrochemical techniques employed in the present work. The results were measured using an Autolab frequency response analyzer (FRA) coupled to an Autolab PGSTAT30 potentiostat/galvanostat with FRA2 module connected to a personal computer, in a three-electrode standard cell system of capacity 100 cm^3.

This cell contains three compartments for working, platinum spiral counter and reference electrodes. A Luggin–Haber capillary was also included in the design. The reference electrode was Ag/AgCl, and used directly in contact with the working solution. The measurements were carried out in aerated uninhibited and inhibited solutions at 70 ◦C and 1.0 bar. For each run, a freshly prepared solution as well as a cleaned set of electrodes was used. Each run was carried out in aerated stirred solutions (using magnetic stirrer) at the cited temperature (±1 ◦C), using a water thermostat.

The linear polarization resistance technique (LPR) was used to study the corrosion inhibition behavior and the polarization resistance, R_p, of the inhibitor film formed on the electrode surface. The LPR curves were recorded in the potential range of -20 to +20 mV with respect to the open circuit potential (OCP) at a scan rate of 0.2 mV s^{-1}. In addition, linear polarization and Tafel plots were used to determine the corrosion potential (E_{corr}) and corrosion current density (j_{corr}) of the corroded and inhibited surfaces. The potentiodynamic polarization curves were recorded in a potential window of -0.25 to 0.25 V vs. E_{corr} at a scan rate of 0.2 mV s^{-1}. Electrochemical impedance measurements were carried out in the frequency range 100 kHz–10 mHz with an amplitude of 5 mV. The aim was to study the charge -transfer (R_{ct}) behavior of the corroded and inhibited surfaces at open circuit potential.

Before each run, the open circuit potential of the working electrode was measured as a function of time during 24 hrs. The order of performing electrochemical measurements was: **(i)** Chronopotentiometry (zero current); OCP *vs.* time (up to 24hrs), followed by **(ii)** LPR technique (E_{corr}

± 20 mV; E_{corr} = steady-state potential in the OCP *vs.* time plots), followed by **(iii)** impedance measurements at E_{corr}, and finally **(iv)** Tafel polarization (E_{corr} ± 250 mV)**.** As the later (i.e., Tafel polarization) is a destructive technique, the cell is cleaned, the test solution is replaced by a fresh one, and a cleaned set of electrodes was used for **(v)** cyclic polarization (CP) measurements.

2.4. Sample Surface analysis

The morphologies of the corroded and inhibited surfaces of the three tested samples were examined by an optical microscope (Metallurgical Microscope MX 7520, Camera Infinity 1, MEIJI TECHNO CO. LTD, JAPAN) and an Analytical Scanning Electron Microscope JEOL JSM 6390 LA. The compositions of such surfaces (inhibited and uninhibited) were determined using ZAF software to quantify the energy-dispersive X-ray spectroscopy (EDS) spectra obtained by an EDS attachment (JEOL EDS EX-54175JMU) on the JEOL SEM. Such morphological examinations were performed after 30 days of immersion in the uninhibited and inhibited solutions at 270 ^{o}C and 29 bar.

3. RESULTS AND DISCUSSION

3.1. Impact of HMoA on corrosion rate

Results of changing the corrosion rate of the tested alloys at different immersion time (up to one month) and the impact of HMoA are presented in Table 2.

Table 2. Average corrosion rates (calculated from mass loss measurements after removal of corrosion products) and the corresponding inhibition efficiency values of the tested amine recorded for the three tested samples in the uninhibited and inhibited solutions as a function of the immersion time at 270 ^{o}C and 29 bar.

Tested Sample	Type of Solution	Average Corrosion Rate (CR / mpy)				Inhibition Efficiency (%)			
		3 days	7 days	14 days	30 days	3 days	7 days	14 days	30 days
A516	Uninhibited	3.1	6.7	15	24	-----	-----	-----	-----
	Inhibited	2.4	5.05	11.2	17	22.58	24.63	25.33	29.17
410 SS	Uninhibited	2.5	5.2	12	18	-----	-----	-----	-----
	Inhibited	1.5	2.2	4.6	6.2	40	57.69	61.67	65.56
304L	Uninhibited	1.32	2.72	5.46	12.95	-----	-----	-----	-----
	Inhibited	0.22	0.35	0.48	0.65	83.33	87.13	91.21	95

Data illustrate that the corrosion rate for A516 and 410SS steadily increases with time, while it is practically stable for 304L. It is shown that presence of HMoA decreases the corrosion rate to an

extent depending on the type of the tested sample and the immersion time. For alloys 410 and 304L, the recorded inhibition efficiency values of the tested HMoA are found to enhance with time, while those recorded in the case of A516 are almost constant. Further analysis of Table 2 reveals that the inhibition performance is always higher, at any given immersion time, in case of 304L; it reached, after 30 days, 95%, 66%, and 30% for 304L, 410SS and A416, respectively. This means that the inhibitor functions well in case of 304L much more than 410 and A516. This may reflect, as will be shown later, the higher adsorption tendency of the tested amine towards the surface of 304L.

3.2. Surface Examinations

Our recently published work [24] showed that the low corrosion resistance of the alloys A516 and 410 SS is reflected in the large amounts of corrosion products formed on their surfaces. On the other hand, the surface of 304L is found to be free from such corrosion products; confirming its high corrosion resistance in these solutions.

In presence of the tested inhibitor, our interest here, the amounts of the corrosion products are reduced and the morphologies of the corroded surfaces improved to an extent depending on the type of the tested sample. A surface film of inhibitor is assumed to be formed, which acts as a barrier to the diffusion of both H^+ and Cl^- ions from solution to electrode surface. These surface events and morphologies are depicted in Figs. 1 and 2.

3.2.1. Light Optical Microscopy

Optical micrographs presented in Fig. 1 show clear difference between the specimens immersed in the uninhibited solution and those immersed in the inhibited one.

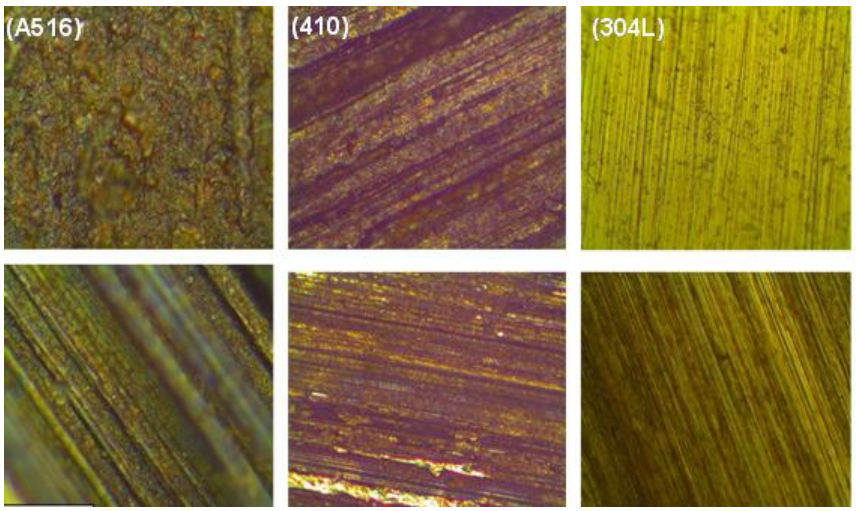

Figure 1. Images of the OM (X200) recorded for the three tested alloys after 30 days of immersion in the uninhibited and inhibited solutions at 270 ^{o}C and 29 bar. Upper images are for the corroded surfaces of A516, SS 410, and SS 304L (without removing corrosion products) [24], while lower ones are for the respective inhibited surfaces.

The specimens immersed in the inhibited solution, particularly alloys A516 and 410 SS, had little corrosion products as compared with those immersed in the uninhibited one, and the polishing marks were still visible.

There were no corrosion products on the inhibited surface of 304L, without any corrosion pits. In comparison, alloys A516 and 410 SS immersed in the uninhibited solution were covered with a layer of corrosion product and pitting was not evident.

3.2.2. SEM/EDX examinations

SEM/EDX examinations of the electrode surface were performed in order to confirm the formation of a protective surface film of inhibitor at the electrode surface. The morphologies of the uninhibited and inhibited surfaces will be discussed after EDX analyses have been presented. For the sake of simplicity, EDX spectra themselves are not included here. However, EDX data that extracted from each EDX spectrum will be discussed here as the atomic percentage (contribution) of each element detected on the electrode surface, based on ZAF Method Standardless Quantitative Analysis, covering the energy range (0 - 20 keV) at 20.0 kV and at a counting rate of 10747 cps. The EDX data were recorded for the three tested samples exposed for 30 days in the uninhibited and inhibited solutions at 270 ^{o}C and 29 bar.

In inhibitor-free solution (uninhibited), the EDX spectra of the three tested samples showed, in addition to the O and Cl, the atomic percentage (contribution) of the alloying elements constituting each tested sample. The presence of the O may be due to the presence of the corrosion products α-FeOOH, Fe_3O_4, γ-Fe_2O_3, and $(Fe,Cr)_3O_4$ [24]. The contribution of Cl refers to the adsorption of Cl^- ions and subsequent formation of $FeCl_2$ phase as one of the corrosion products (inspect XRD; Figs. 8a and 8b in *Ref.* [24]). On the other hand, in the inhibited solution, the EDX spectra showed additional contribution characteristic for the existence of N due to the adsorption of amine. In addition, the contribution of C enhanced as a result of the C atoms of the adsorbed amine molecules.

This data show that a carbonaceous material containing N has covered the electrode surface. This layer is undoubtedly due to the inhibitor, because of the detection of the N atom and the high contribution of the C observed in presence of additives. The N atom and the high contribution of the C atoms are not present on the electrode surface exposed to the uninhibited solution. Further inspection of the EDX data revealed that the contribution of Fe, Cl, O and some of the alloying elements were suppressed relative to the samples exposed to the uninhibited solution because of the overlying inhibitor film, which protects steel against corrosion.

It should be noted that the contribution of C and N atoms as well as the suppression observed in the contribution of Fe, Cl and O atoms depend on the type of the tested sample. These events are always significant in case of 304L, confirming the results of the autoclave tests that the inhibition performance of the tested amine is always high on the surface of 304L.

Figure 2 shows three arrays (A, B, and C) of SEM images recorded for the tested samples exposed for 30 days in the uninhibited and inhibited solutions at 270 ^{o}C and 29 bar. Array (A) is the SEM images of the three tested samples before removal of corrosion products [24]. While the

corrosion deposits accumulate on the surfaces of the carbon steel sample (A516) and the ferritic stainless steel sample (410), the surface of the austenitic stainless steels (304L) is free from corrosion products, as shown in array (A). After the corrosion deposits have been removed, array (B), rough surfaces of A516 and 410 are visualized which can be associated to the aggressiveness of the uninhibited solution. This surface roughness obviously decreases on going from A516 to 304L [24].

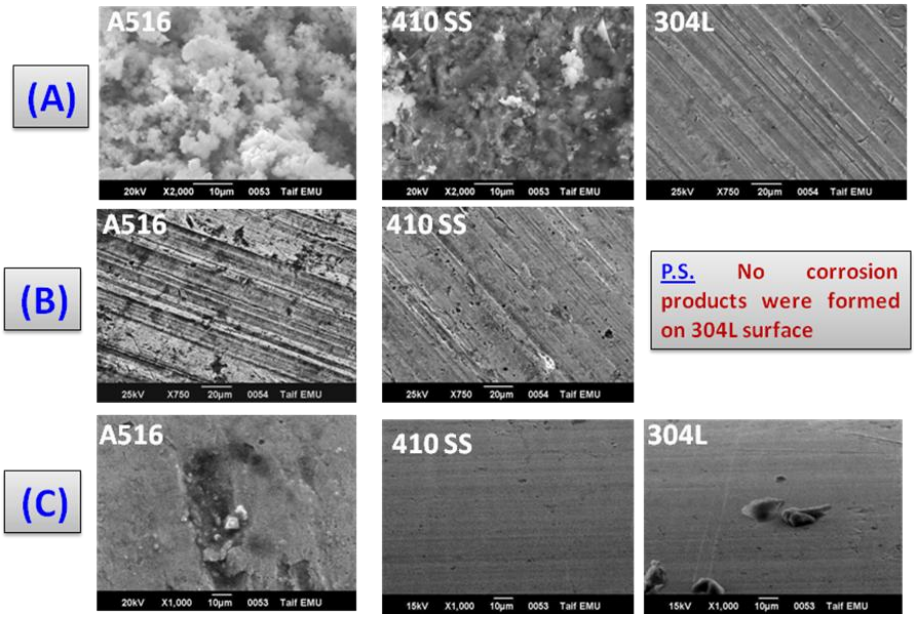

Figure 2. SEM images recorded for the three tested samples after 30 days of immersion in the uninhibited and inhibited solutions at 270 ^{o}C and 29 bar. (A): before corrosion products removal [24] (B): After the corrosion products have been removed [24] (C): In presence of the tested amine (the inhibitor)

Conversely, when the tested samples are immersed in the inhibited solution, array (C), surface morphologies are found to be improved to an extent depending on the type of the tested sample. This improvement in surface morphology is due to the decrease in the corroded areas caused by the inhibitor layer covering the electrode surface. Significant improvement in the surface morphology is again observed in case of 304L much more than 410 SS and A516.

3.3. Electrochemical tests

3.3.1. OCP vs. time measurements

Measuring the variation with time of the OCP of the working electrode is important in defining domains of corrosion, partial and complete inhibition, and in determining inhibitor-threshold concentrations [26]. Potential measurements during 24h showed different features of these curves deserve comments. It has been noticed in all cases that, as will be seen and fully discussed, the effective events have occurred within the first 60 min of immersion in the uninhibited and inhibited

solutions; the reasons we only discussed the variation of the OCP with time during the first 60 min of immersion, as shown in Figs. 3a-3c.

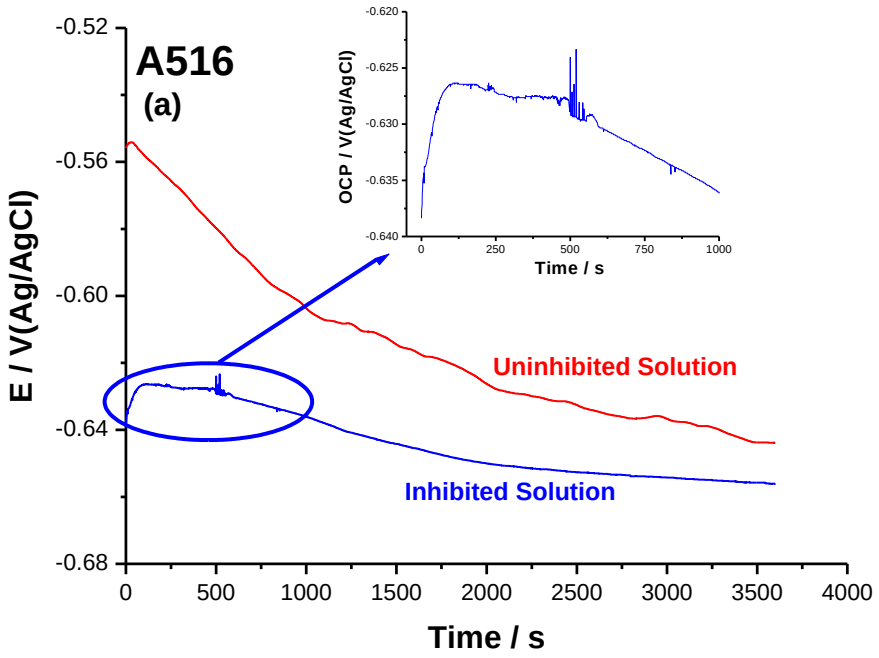

Figure 3(a). OCP vs. time (up to 24 hrs) plots recorded for sample A516 in the uninhibited and inhibited solutions at 70 ^{o}C and 1.0 bar.

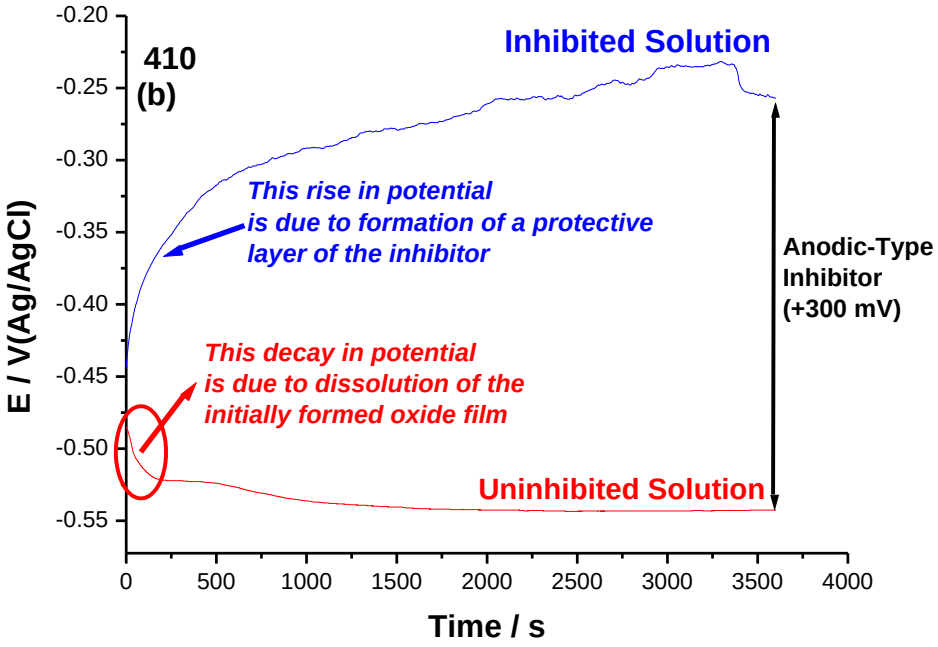

Figure 3(b). OCP vs. time (up to 24 hrs) plots recorded for sample 410 SS in the uninhibited and inhibited solutions at 70 ^{o}C and 1.0 bar.

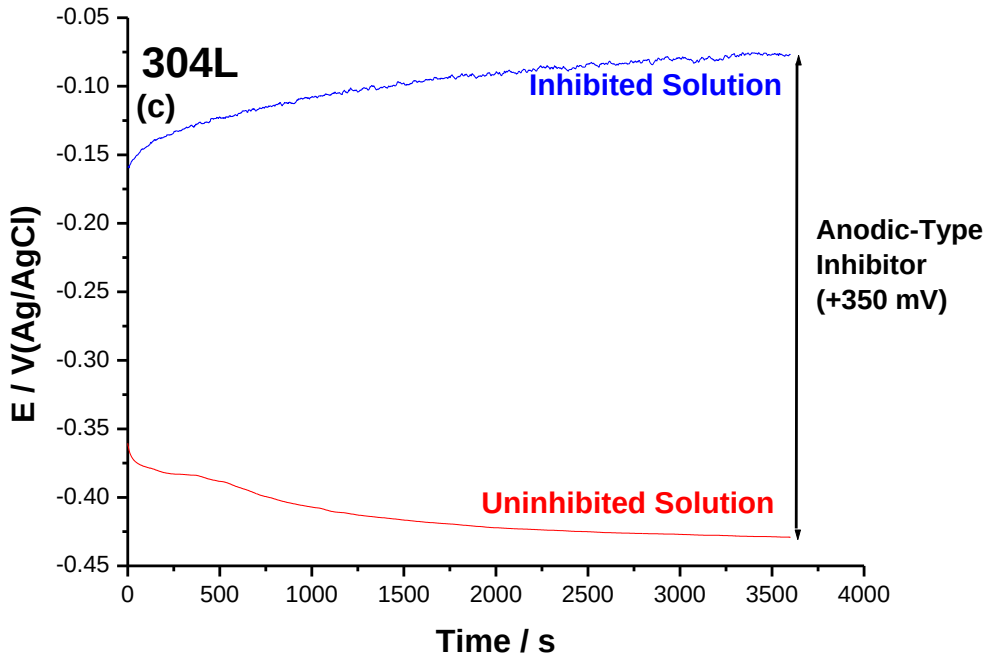

Figure 3(c). OCP vs. time (up to 24 hrs) plots recorded for sample 304L in the uninhibited and inhibited solutions at 70 ^{o}C and 1.0 bar.

In LAO bulk solution, it can be seen, for the three tested alloys, that the OCP changed quickly towards more negative values, indicating the initial dissolution process of the pre-immersion, air formed oxide film and the attack on the bare metal [27]. A steady potential was readily attained, corresponding to the free corrosion of the metal [26].

Comparison of the carbon steel (A516) with the two tested stainless steels (410 and 304L) shows that the obtained immersion potential (E_{ocp} at t = 0) and the steady-state E_{corr} values of A516 are always more negative. In addition, carbon steel A516 needs longer times from electrode immersion to reach steady-state. This means that the surface of A516 is subjected to corrosion more than 410 and 304L, which stabilize readily in these solutions; shorter times are required for these materials to reach steady-state.

The active corrosion of A516 could be attributed, as previously discussed [24], to the acceleration influence of the galvanic cells created by the ferrite and the pearlite grains, which are in contact with each other in the microstructure of A516. The more negative steady-state E_{corr} potential values of A516 suggest that the presence of the ferrite and the pearlite grains influences the kinetics of the cathodic reaction [24].

On the other hand, in the presence of HMoA, the OCP shifted first to less negative values reaching a maximum, as in the case of alloy A516 (Fig. 3a). After a certain time, the potential declined to a reasonably steady value. This trend indicated the occurrence of two counter-acting processes. The first process being the formation of a protective layer of the inhibitor on the electrode surface, and

consequently delayed-action corrosion occurred shifting the OCP to nobler values. The second process is corrosion, which dragged the potential back towards active values.

The competition between these two counter-acting processes may explain the appearance of the arrest depicted in Fig. 3a. These results indicate that the tested amine, in this case, is unable to ensure permanent-corrosion inhibition. These results confirm the poor adsorption tendency (i.e., low inhibition performance) of the tested HMoA on the surface of A516. The little shift in the steady state OCP (i.e., the corrosion potential E_{corr}) upon inhibitor addition (Fig. 3a) reveals that the tested amine acts as a mixed-type inhibitor on the surface of A516.

However, adsorption of the inhibitor on the surfaces of 410 and 304L prevented the decay of potentials to negative values, (Figs. 3b and 4c), confirming the high adsorption affinity of the tested amine on the surfaces of the two tested stainless steels. The significant noble shift (> +300 mV) of the steady state OCP recorded for the inhibitor action on the surfaces of 410 and 304L (Figs. 3b and 4c) may be explained on the basis that the inhibitor adsorbs preferentially on the electrode surface impeding the anodic sites, a typical anodic-type inhibitor.

3.3.2. LPR measurements

For linear polarization (LP) measurements, a sweep from -20 to +20 mV *vs.* OCP at a scan rate of 0.20 mV s^{-1} was used and the polarization resistance (R_p) was measured from the slope of the LP plot (*E vs. j* curve in the vicinity of corrosion potential; data not shown here). Since the electrochemical theory assumes that R_p^{-1} is directly proportional to the corrosion rate, the inhibition efficiencies, I_{LP}(%), of the tested amine towards corrosion of A516, 410 and 304L were calculated from (R_p) values, using Eq. (1):

$$I_{LP}(\%) = 100 \times \{(R_p) - (R^o_p) / (R_p\} \qquad (1)$$

where R^o_p and R_p are the polarization resistance values without and with the addition of HMoA, respectively. For the three tested samples, the polarization resistances (R_p) were found to increase when HMoA is added to the uninhibited solution, corresponding to increased corrosion resistance. Higher values of R^o_p, R_p, and I_{LP}(%) were obtained for 304L, even in absence of inhibitor. The calculated inhibition efficiencies, based on Eq. 1, are found to increase from 75% for A516 to 94.5% and 98.7 % 410 and 304L, respectively. These findings support previous results that: (i) 304L is the highest corrosion resistant among the tested samples and (ii) the inhibition performance of the tested amine towards corrosion of 304L is higher than its inhibitive characteristics towards corrosion of A516 and 410.

3.3.3. Tafel polarization measurements

The uniform corrosion behaviour and the nature of the inhibition process were also established on the basis of Tafel polarization measurements. Thus, changes observed in the polarization curves after inhibitor addition are usually used as criteria to classify the inhibitor as cathodic, anodic or mixed

[28]. In addition, Tafel polarization measurements were performed in order to verify the correlation with OCP *vs.* time measurements and chemical tests.

Figures 4 and 5a-5c illustrate the cathodic and anodic polarization curves recorded for the three tested samples in the uninhibited and inhibited solutions at 70 ^{o}C and 1.0 bar.

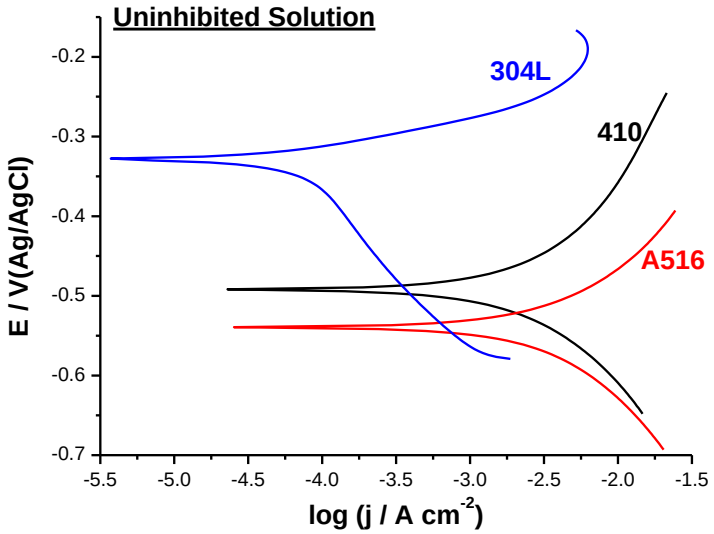

Figure 4. Tafel plots recorded for the three tested samples the uninhibited solution at 70 ^{o}C and 1.0 bar.

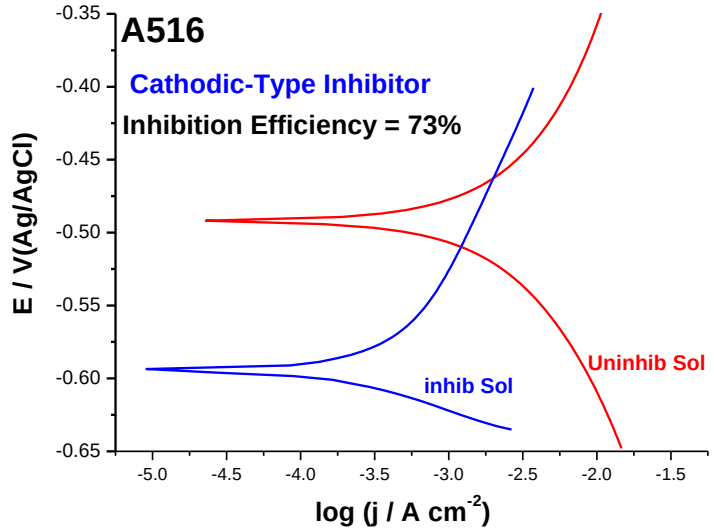

Figure 5(a). Tafel plots recorded for sample A516 in the uninhibited and inhibited solutions at 70 ^{o}C and 1.0 bar.

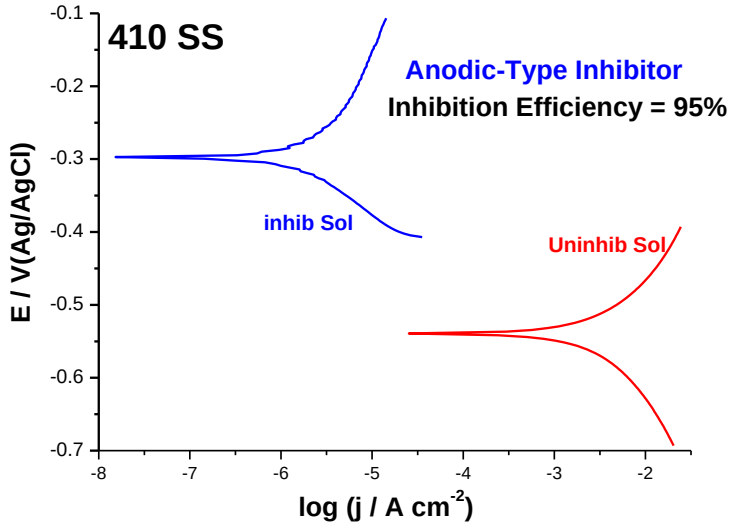

Figure 5(b). Tafel plots recorded for sample 410 SS in the uninhibited and inhibited solutions at 70 ^{o}C and 1.0 bar.

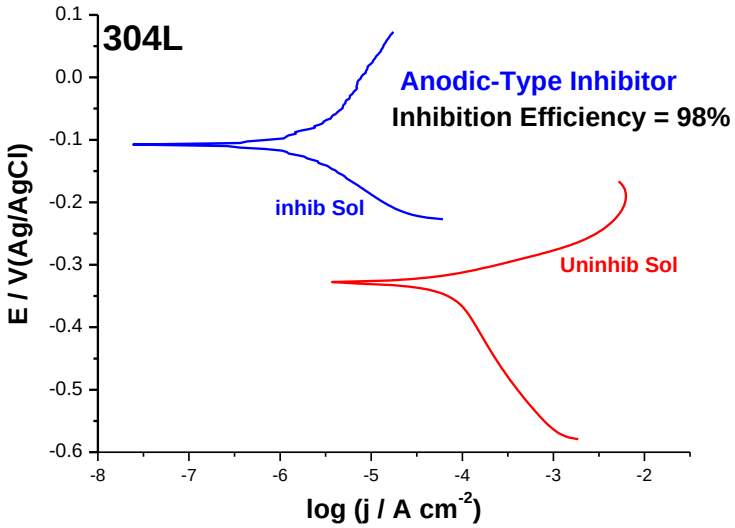

Figure 5(c). Tafel plots recorded for sample 304L in the uninhibited and inhibited solutions at 70 ^{o}C and 1.0 bar.

The modifications caused by the tested amine when it adsorbs on the corroded surfaces of 410 and 304L (Figs. 5b and 5c) are a significant positive shift in the corrosion potential (E_{corr}), in the direction of what was seen by means of OCP *vs.* time plots (Fig. 3a-3c), and a marked decrease in the current density of both anodic and cathodic polarization curves. The reverse has been observed during the corrosion inhibition of A516 (Fig. 5a); a marked negative shift in E_{corr}, in the direction of what was exactly observed in the OCP *vs.* time plots (Fig. 3a) and an obvious decrease in the cuurent density of the cathodic branch.

In all cases it has been shown that the cathodic and anodic overpotentials increase (i.e., the rates of the cathodic and anodic reactions are retarded) upon introducing the inhibitor to an extent depending on the type of the tested sample. Based on these observations, the tested amine is considered to act, in all cases, as a mixed-type inhibitor, but with an anodic predominance for 410 and 304L and a cathodic predominance for A516.

The linear Tafel segments of the cathodic and anodic curves were extrapolated to the corrosion potential to obtain the corrosion current densities (j_{corr}). Since the corrosion rate is directly proportional to the value of the corrosion current density, the inhibition efficiency, I_{Tafel}(%), of the tested amine was evaluated from the measured j_{corr} values using the relationship:

$$I_{Tafel}(\%) = 100 \times \{(j^{o}_{corr}) - (j_{corr}) / (j^{o}_{corr})\} \qquad (2)$$

where j^{o}_{corr} and j_{corr} are the corrosion current densities for uninhibited and inhibited solutions, respectively. Here again, the highest inhibition efficiency of the tested amine is recorded on the surface of 304L; the calculated inhibition efficiencies are found to be 73%, 93%, and 98% for A516, 410, and 304L, respectively.

3.3.4. Impedance measurements

Figures 6a-6c represent complex-plane, Bode, and phase angle impedance plots recorded for 304L (as a representative example) in the uninhibited and inhibited solutions at 70 ^{o}C and 1.0 bar and at the respective corrosion potentials. Similar findings were recorded for the other tested alloys A516 and 410; data not included here. It follows that a depressed charge-transfer semicircle is observed, due to the time constant of charge transfer and double-layer capacitance [29–31].

This semicircle makes an angle approaching 50◦ with the real axis and its intersection defines the solution (R_s) enclosed between the working electrode and the counter electrode. The corrosion behaviour of the three tested steel alloys and the inhibition performance of amine can be evaluated by the diameter of the semicircle (the charge-transfer resistance, R_{ct}), double layer capacitance (C_{dl}) and the maximum phase angle (θ_{max}) of the impedance.

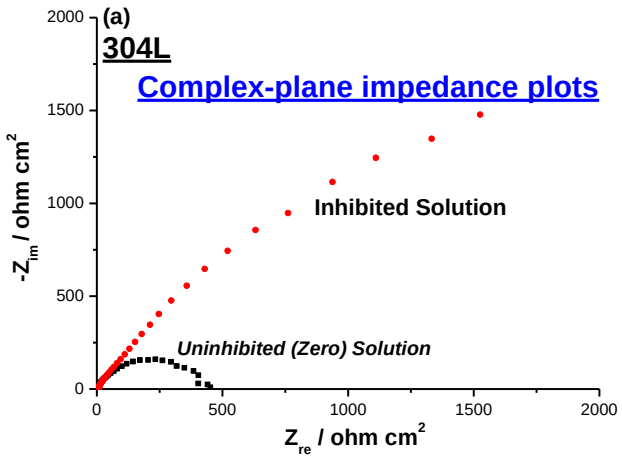

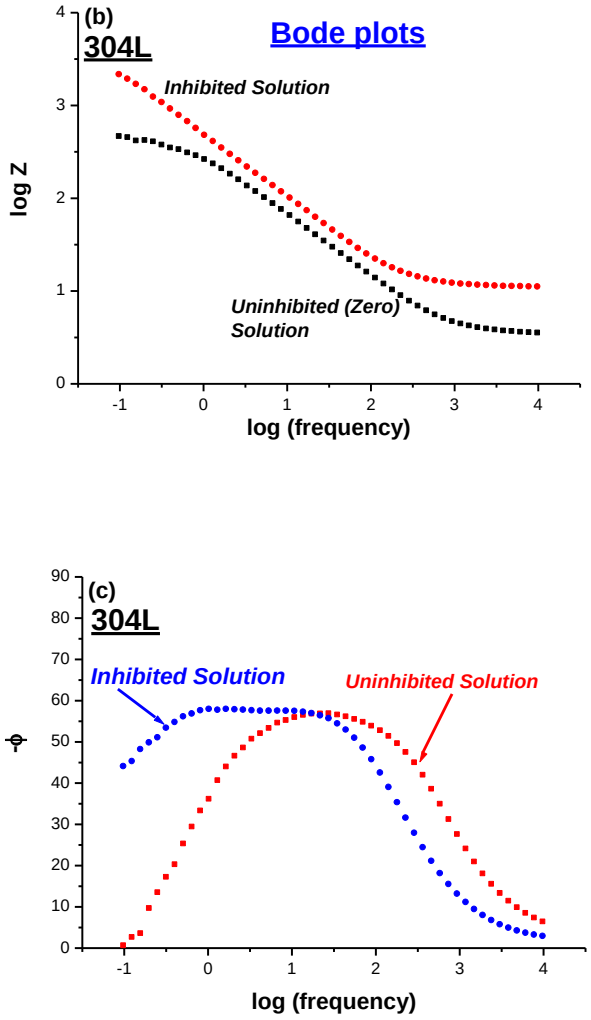

Figure 6. Complex-plane impedance (a), Bode (b), and Phase angle (c) plots recorded for sample 304L in the uninhibited and inhibited solutions at 70 ^{o}C and 1.0 bar.

The more densely packed the monolayer of the inhibitor, the larger the diameter of the semicircle, which results in higher R_{ct} and lower C_{dl} values. A large R_{ct} is associated with a slower corroding system [32]. Furthermore, a better protection provided by an inhibitor is associated with a decrease in C_{dl} [32]. The decrease in C_{dl}, which results from a decrease in local dielectric constant and/or an increase in the thickness of the electrical double layer due to inhibitor adsorption [33].

It is well known that the maximum phase angle (θ_{max}) should be 90◦ for a corrosion interface represented by a simple R−C parallel equivalent circuit when R_s = 0. However, depressed semicircles are usually obtained for practical electrode/solution interface, which has been known to be associated with the roughness of electrode surface. In the present work, rough surfaces were obtained as a result of the aggressive attack of HCl on the surfaces of the tested samples, as evidenced from OM and SEM examinations (Figs. 1 and 2). This aggressive attack reduces the value of θ_{max}. A less depressed semicircle (with higher maximum phase angles close to 90◦) also indicates a better quality of the inhibitor monolayer.

Results of the present work showed that the values of R_{ct} and θ_{max} increase, while those of C_{dl} tend to decrease when amine is added to the corrosive environment, reflecting its inhibitive characteristics. Values of R_{ct} and θ_{max} are always higher, while those of C_{dl} are always lower in case of 304L, irrespective of the absence or presence of the tested amine. This is clearly seen in Fig. 7, which represents the results of R_{ct} for the three tested alloys in the uninhibited and inhibited solutions at 70 ^{o}C and 1.0 bar.

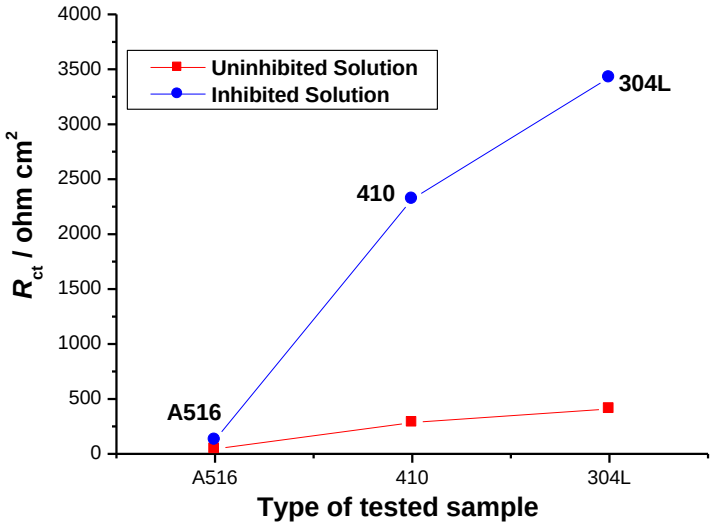

Figure 7. Charge-transfer resistance (R_{ct}) as a function of the type of the tested sample at 70 ^{o}C and 1.0 bar.

The highest value of inhibition efficiency, about 96%, (obtained using an equation similar to Eq. 1, after replacing R_p by R_{ct}) was also recorded, as expected, for 304L. These findings confirm previous ones that 304L is the best from the corrosion and corrosion control points of view among the tested samples.

3.3.5 Passivity and passivity breakdown (Cyclic polarization (CP) measurements)

As previously shown, Tafel plots provided us with general corrosion rate information of the three tested alloys with a 400 to 500 mV potential range. The amount of information obtained from electrochemical corrosion measurements increased, as wider polarization potential ranges are used to generate the data. CP measurements are generated with approximately 1250 mV to 4000 mV potential ranges, and provide additional information concerning corrosion kinetics, passivity, and localized corrosion of the tested samples.

Figure 8a depicts cyclic polarization curves (linear scale) recorded for 304L (as a representative example) in the uninhibited and inhibited solutions at 70 ^{o}C and 1.0 bar. Similar behaviour was obtained for A516 and 410 (data not included here).

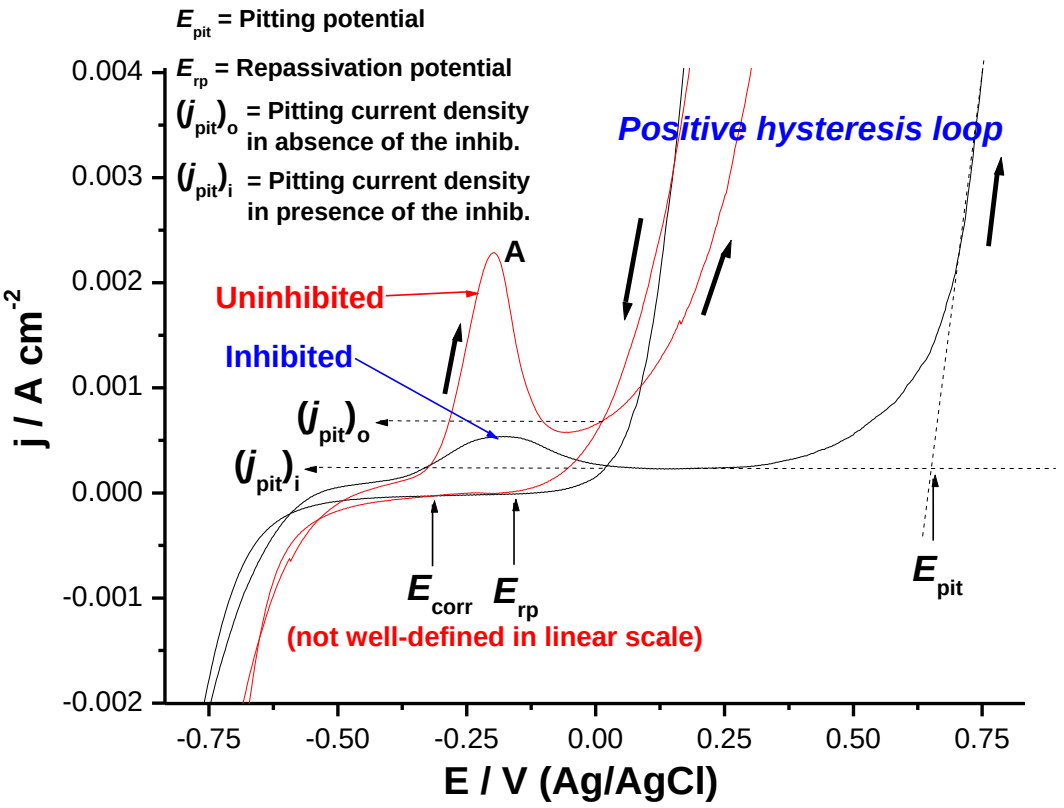

Figure 8(a). Cyclic polarization plots (linear scale) recorded for sample 304L in the uninhibited and inhibited solutions at 70 ^{o}C and 1.0 bar.

As the electrode potential was made increasingly positive, the anodic polarization curves exhibit an active/passive transition. In the active region, the dissolution current density increases linearly with the applied potential. This is followed by the appearance of the anodic peak A. The active dissolution of the anode is due to the formation of (Fe-aggressive anion) soluble complex species. The decay in the active dissolution current density is related to the formation of a protective oxide film. Therefore, the appearance of peak A is indicative of two processes; metal dissolution and subsequent formation of soluble complex species and the formation of a protective passive film.

The anodic dissolution current density drops to a very small value, designated as passive current (j_{pass}), indicating the onset of passivation. The value of j_{pass} is limited by the chemical dissolution of the film. The chemical film dissolution is counterbalanced by film formation. The rates of these two processes are nearly the same at the steady-state of polarization so as to keep the thickness of the passive film nearly constant. However, it seems that the aggressive Cl^- ions did not give the change for a real passive region to form and extend. Once the anodic dissolution current density of peak A drops to its very small value to start passivation, passivity breakdown and localized attack occurs at a certain critical potential, known as the pitting potential (E_{pit}). The mechanism of passivity breakdown and initiation of stable pits by chlorides is well documented in the literature.

Passivity breakdown and initiation of pitting are evident by the sudden increase in j_{pass} at E_{pit}. It is obvious that pitting continues even after potential scan reversal, because the pitting attack is enhanced after the pit initiation (autocatalytic character of pitting) [34]. A positive current hysteresis loop, characteristic of pitting corrosion phenomena, appears. Positive hysteresis occurs when passive film damage is not repaired and/or pits initiate. Generally, the existence of a hysteresis loop in a cyclic potentiodynamic polarization curve indicates a delay in repassivation of an existing pit when the potential is scanned toward negative direction. The larger the hysteresis loop, the more difficult it becomes to repassivate the pit [34]. This loop allows the repassivation potential (E_{rp}) to be determined [34].

The location of E_{rp} with respect to E_{corr} is well-defined in the corresponding log j vs E plot (Fig. 8b).

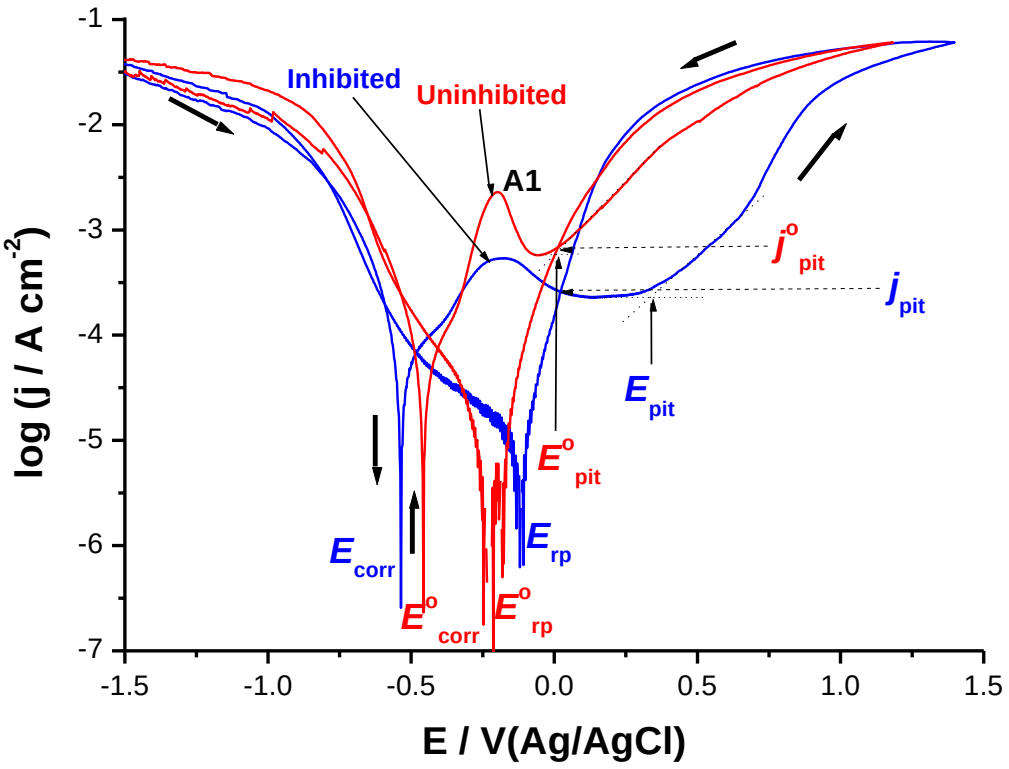

Figure 8(b). Cyclic polarization plots (logarithmic scale) recorded for sample 304L in the uninhibited and inhibited solutions at 70 °C and 1.0 bar.

In the present work, E_{rp} is defined as the potential on the reverse scan at which the anodic current becomes zero (i.e., the current changes polarity); the pitting current in the reverse scan decreases and completely suppressed at E_{rp}, where pit growth is arrested [35]. At potentials more negative than E_{rp}, the electrode is protected by an oxide film and pitting will only take place at more positive potentials [34].

This hysteresis anodic loop denotes that the electrode was able to repassivate after the breakdown of the passive film. The anode finds it easy to repassivate since the repassivation potential

(E_{rp}) locates anodic to E_{corr}, resulting in a small hysteresis loop. The intersection of the reverse current with the forward one defines what is called pitting current (j_{pit}), which is a measure for the rate of pitting corrosion.

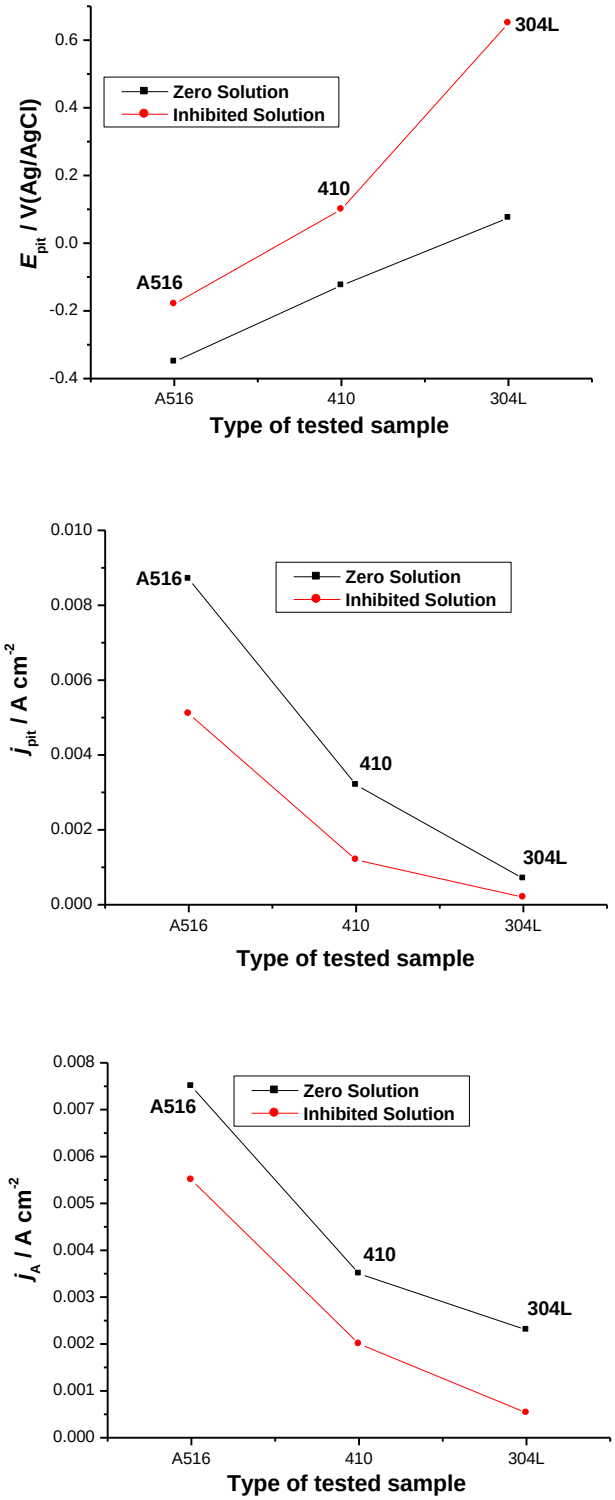

Figure 9. Pitting potential (E_{pit}), pitting current density (j_{pit}) and height of the anodic peak A (j_A) as a function of the type of the tested sample.

The anodic peak height (current), j_A, and the pitting corrosion parameters, namely E_{pit} and j_{pit} were found to depend on solution composition and type of tested alloy; Fig. 9 summarizes such events.

On the other hand, E_{rp} is found to be independent of solution composition and type of tested alloy. Referring to Fig. 9, for any tested alloy, higher values of E_{pit} and lower j_{pit} and j_A values were recorded in presence of the tested amine (the inhibited solution). A film of the inhibitor is assumed to be formed on the electrode surface, protecting it against corrosion.

Irrespective of the absence or presence of the inhibitor, higher values of E_{pit} and lower j_{pit} and j_A values were obtained for 304L, compared with those recorded for A516 and 410 alloys. These results confirm previous findings that 304L possesses the highest corrosion resistance among the tested alloys.

4. PROPOSED INHIBITION MECHANISMS

The steel surface in acidic medium contains anodic and cathodic sites, derived from the simultaneous electrochemical reaction of hydrogen evolution and iron oxidation.

4.1. Anodic sites

The adsorption and desorption of the aggressive Cl^- ions occur on the anodic sites, and subsequent iron dissolution (as Fe^{2+}) takes place following the reactions explained in [36]. In our recently published study [24], XRD confirmed the existence of $FeCl_2$ as one of the corrosion products formed on the surfaces of A516 and 410. The tested inhibitor is an organic base, which can be protonated in presence of HCl. Thus, it becomes a cation, existing in equilibrium with the corresponding molecular form as the following:

$$HMoA + HCl \leftrightarrow HMoAH^+ + Cl^- \quad (3)$$

The Cl^- ions are first adsorbed at the steel/solution interface at the corrosion potential through electrostatic attraction force due to the excess positive charge at the steel/solution interface [14,37-39], followed by $(FeCl^-)_{ads}$ species formation [36].

We propose here that the adsorbed species $(FeCl^-)_{ads}$ interact with the cations of $HMoAH^+$ forming an adsorptive protective film of electrostatic character, with a consequent reduction in corrosion rate as a result of blocking active sites on the alloy surface.

The anodic reactions, in the presence of the corrosion inhibitor HMoA, may be summarized as follows:

$$Fe + Cl^- \leftrightarrow (FeCl^-)_{ads} \quad (4)$$

$$(FeCl^-)_{ads} + HMoAH^+ \rightarrow (FeCl^- HMoAH^+)_{ads} \quad (5)$$

4.2. Cathodic sites

The adsorption of H^+ and desorption of H_2 occurs concurrently on the cathodic sites [36]. The protonated HMoA molecules are expected to electrostatically adsorb on the cathodic sites in competition with H^+, reducing the rate of the hydrogen evolution reaction.

Following Likhanova et. al [36], the cathodic reactions, in the absence of corrosion inhibitor,

may be summarized as: formation of FeH^+ and FeH. Accordingly in the presence of HMoA, the following reactions occurred:

$$Fe + HMoAH^+ \leftrightarrow Fe(HMoAH^+)_{ads} \quad (6)$$

$$Fe(HMoAH^+)_{ads} + e^- \rightarrow (FeHMoAH)_{ads} \quad (7)$$

4.3. Possibility of chemical adsorption via coordination

In addition to the physical adsorption, there should be chemical adsorption, which involves charge sharing or charge-transfer from the inhibitor molecules to the metal surface to form a coordinate type of a bond. The presence of a transition metal, having vacant and low-energy electron orbitals and of an inhibitor with molecules having relatively loosely bound electrons or heteroatoms with a lone pair of electrons, is necessary. Effective inhibition is predominantly provided by the direct coordination of un-protonated N atom to metal atoms. Iron {[Ar] $4s^2$ $3d^6$} is a member of a group in the 3d transition series. Its chemistry, in general, is determined strongly by the electron exchange between the partly filled d-shells and electron donors or acceptors from the environment.

Coordinate bonds are expected to form between the active centers (the lone electron pairs of the nitrogen atom of the amino group) of the unprotonated inhibitor molecule and the empty orbitals of iron atoms. This results in the formation of a chemisorbed protective layer. In addition, cations of EHA may accept electrons from the metallic surface to reach electroneutrality [36], this way chemisorption occurs by a retro-donation mechanism, resulting in the formation of a chemisorbed protective layer.

4.4. Possibility of chemical adsorption via H-bonding

The XRD patterns of our previous study [24] revealed the presence of the oxides Fe_2O_3, Fe_3O_4 and $(Fe,Cr)_3O_4$ due to corrosion. The presence of oxides on the electrode surface may promote inhibitor adsorption via hydrogen bonding [40-42]. Adsorption in this case is assisted by hydrogen bond formation between amine and the oxidized surface species (corrosion products). This type of adsorption should be more prevalent for protonated N-atom, because the positive charge on N-atom is conductive to the formation of hydrogen bonds. Adsorption by direct chemisorptions for un-protonated N-atom may also occur, as previously discussed, on an exposed metal atom. The extent of adsorption by the respective modes depends on the nature of the metal surface.

Effective inhibition is predominantly provided by the direct coordination of un-protonated N-atom to metal atoms. In presence of the oxide film, although the protonated and un-protonated N-atom can interact with oxidized metal and the corrosion intermediates by hydrogen bonding, little is

contributed to corrosion inhibition because corrosion intermediates and surface oxides could not form a stable compact layer on the metal surface, as in the case of our tested carbon steel A516.

However, the presence of $(Fe,Cr)_3O_4$ phase in the oxide layer structure of the tested stainless steels 410 and 304L [24] will make the oxide film, as previously discussed, more compact and protective, which in turn stabilizes the adsorption by H-bond. This may explain why the tested amine functions well (i.e., possesses a high adsorption affinity) on the surfaces of 410 and 304L more than on A516 surface. In this respect, we are not surprising why the highest protection efficiency of the tested amine is recorded for 304L. This is undoubtedly due to its high Cr and Ni contents. Cr promotes the formation of a protective surface oxide and Ni enhances the stability of the protective oxide [43].

5. CONCLUSION

In view of the above discussion and investigations, the followings can be concluded:

(i) Tested HMoA did not increase corrosion rate of tested carbon steel, ferritic and austenitic stainless steel in LAO solution.

(ii) The inhibition performance of the tested HMoA towards corrosion of 304L is always higher, as compared with 410 and A516.

(iii) Surface examinations of the corroded and inhibited surfaces (using OM, SEM/EDX, and AFM) showed that the roughness of the surfaces of the three tested samples decreases following the order: A516 < 410 << 304L.

(iv) Efficiency of the HMoA was confirmed with results of carried out electrochemical measurements.

(v) Generally, HMoA retarded intensity of both electrochemical reactions (cathodic and anodic) and can be classified as a mixed type inhibitor, but with an anodic predominance for 410 and 304L and a cathodic predominance for A516.

(vi) The most probable mechanism of investigated HMoA is explained with physical and chemical adsorption.

(vii) Higher efficiency for stainless steel is explained with presence of H bond between amine fragment in HMoA and oxidized surface containing $(Fe,Cr)_3O_4$ phase.

References

1. J.H. Potgieter, P.A. Olubambi, L. Cornish, C.N. Machio, El-Sayed M. Sherif, *Corros. Sci.*, 50 (2008) 2572, and references therein.
2. I.A. Kartsonakis, A.C. Balaskas, E.P. Koumoulos, C.A. Charitidis, G.C. Kordas, *Corros. Sci.*, 57 (2012) 30.
3. M. Sababi, J. Pan, P.-E. Augustsson, P.-E. Sundell, P.M. Claesson, *Corros. Sci.*, 84 (2014) 189.
4. M. Behzadnasab, S.M. Mirabedini, M. Esfandeh, *Corros. Sci.*, 75 (2013) 134.
5. A.-M. Lazar, W.P. Yespica, S. Marcelin, N. Pébère, D. Samélor, C. Tendero, C. Vahlas, *Corros. Sci.*, 81 (2014) 125.
6. W.-G. Zhang, L. Li, S.-W. Yao, G.-Q. Zheng, *Corros. Sci.*, 49 (2007) 654.
7. Y. González-García, S. González, R.M. Souto, *Corros. Sci.*, 49 (2007) 3514.

8. A. Márquez-Herrera, J.L. Fernandez-Muñoz, M. Zapata-Torres, M. Melendez-Lira, P. Cruz-Alcantar, *Surf. & Coat. Technol.*, 254 (2014) 433.
9. J. Jiang, Y. Wang, Q. Zhong, Q. Zhou, L. Zhang, *Surf. & Coat. Technol.*, 206 (2011) 473.
10. M. Barbalat, D. Caron, L. Lanarde, M. Meyer, S. Fontaine, F. Castillon, J. Vittonato, Ph. Refait, *Corros. Sci.*, 73 (2013) 222.
11. X. Chen, X.G. Li, C.W. Du, Y.F. Cheng, *Corros. Sci.*, 51 (2009) 2242.
12. Ph. Refait, M. Jeannin, R. Sabot, H. Antony, S. Pineau, *Corros. Sci.*, 71 (2013) 32.
13. L.Y. Xu, Y.F. Cheng, *Corros. Sci.*, 78 (2014) 162.
14. M. Finšgar, J. Jackson, *Corros. Sci.*, 86 (2014) 17, and references therein.
15. M.A. Amin, S.S. Abd El-Rehim, E.E.F. El-Sherbini, R.S. Bayoumi, *Electrochim. Acta* 52 (2007) 3588.
16. H.H. Hassan, E. Abdelghani, M.A. Amin, *Electrochim. Acta* 52 (2007) 6359.
17. M.A. Amin, S.S. Abd El-Rehim, E.E. F. El-Sherbini, R.S. Bayoumi, *Int. J. Electrochem. Sci.* 3 (2008) 199.
18. M.A. Amin, *Jordan J. Chem.* 5 (2010) 371.
19. M.A. Amin, G.A.M. Mersal, Q. Mohsen, *Arabian J. Chem.* 4 (2011) 223.
20. M.A. Amin, M.A. Ahmed, H.A. Arida, T. Arslan, M. Saracoglu, F. Kandemirli, *Corros. Sci.* 53 (2011) 540.
21. M.A. Amin, M.A. Ahmed, H.A. Arida, F. Kandemirli, M. Saracoglu, T. Arslan, *Corros. Sci.* 53 (2011) 1895.
22. M.A. Amin, M.M. Ibrahim, *Corros. Sci.* 53 (2011) 873.
23. M.A. Amin, O.A. Hazzazi, F. Kandemirli, M. Saracoglu, *Corrosion* 68 (2012) 688.
24. M.A. Amin, Q. Mohsen, N.Y. Mostafa, N. El-Bagoury, A. Al-Refaie, A.K. Bairamov, S. Al-Maaesab, E. Morales Murillo, S.A. Al-Qahtani, *Int. J. Electrochem. Sci.* 9 (2014) 2631.
25. ASTM G1-03 "Standard Practice for Preparing, Cleaning, and Evaluating Corrosion Test" (2011).
26. A.M. Shams El Din, R.A. Mohammed, H.H. Haggag, *Desalination* 114 (1997) 85.
27. U.R. Evans, The Corrosion of Metals, Edward Arnold, London, 1960, p. 898.
28. B.G. Cubley (Ed.), Chemical Inhibitors for Corrosion Control, The Royal Society of Chemistry, 1990.
29. S.S. Abdel Rehim, H.H. Hassan, M.A. Amin, *Appl. Surf. Sci.* 187 (2002) 279.
30. O.E. Barcia, O.R. Mattos, N. Pebere, B. Tribollet, *J. Electrochem. Soc.* 140 (1993) 2825.
31. C. Deslouis, B. Tribollet, G. Mengoli, M.M. Musiani, *J. Appl. Electrochem.* 18 (1988) 374.
32. D.A. Lopez, S.N. Simison, S.R. de Sanchez, *Electrochim. Acta* 48 (2003) 845.
33. W.J. Lorenz, F. Mansfeld, *Corros. Sci.* 21 (1981) 647.
34. Z. Szklarska-Smialowska, Pitting Corrosion of Metals, NACE, Houston, TX, 1986.
35. M. Finsgar, S. Fassbender, S. Hirth, I. Milosev, *Mater. Chem. & Phys.* 116 (2009) 198.
36. N.V. Likhanova, M.A. Dominguez-Aguilar, O. Olivares-Xometl, N. Nava-Entzana, E. Arce, H. Dorantes, *Corros. Sci.* 52 (2010) 2088.
37. L.I. Antropov, E.M. Makushin, V.F. Panasenko, Metal Corrosion Inhibitors, Kiev, Technika, 1981.
38. O.E. Barcia, O.R. Mattos, N. Pebere, B. Tribollet, *J. Electrochem. Soc.* 140 (1993) 2825.
39. A. Lukomska, J. Sobkowski, *J. Electroanal. Chem.* 567 (2004) 95.
40. M.J. Incorvia, S. Contarini, *J. Electrochem. Soc.* 136 (1989) 2493.
41. F.H. Karman, I. Felhosi, E. Kalman, I. Cserny, L. Kover, *Electrochim. Acta* 43 (1998) 69.
42. R.D. Braun, E.E. Lopez, D.P. Vollmer, *Corros. Sci.* 34 (1993) 1251.
43. X. Gao, X. Wu, Z. Zhang, *J. Supercritical Fluids* 42 (2007) 157.